Catalysis Science & Technology

ROYAL SOCIETY OF CHEMISTRY

PAPER

View Article Online
View Journal | View Issue

Cite this: *Catal. Sci. Technol.*, 2021, **11**, 6832

Revisiting trends in the exchange current for hydrogen evolution†

Timothy T. Yang,[a] Rituja B. Patil,[b] James R. McKone[b] and Wissam A. Saidi*[a]

Nørskov and collaborators proposed a simple kinetic model to explain the volcano relation for the hydrogen evolution reaction on transition metal surfaces such that $j_0 = k_0 f(\Delta G_H)$ where j_0 is the exchange current density, $f(\Delta G_H)$ is a function of the hydrogen adsorption free energy ΔG_H as computed from density functional theory, and k_0 is a universal rate constant. Herein, focusing on the hydrogen evolution reaction in acidic medium, we revisit the original experimental data and find that the fidelity of this kinetic model can be significantly improved by invoking metal-dependence on k_0 such that the logarithm of k_0 linearly depends on the absolute value of ΔG_H. We further confirm this relationship using additional experimental data points obtained from a critical review of the available literature. Our analyses show that the new model decreases the discrepancy between calculated and experimental exchange current density values by up to four orders of magnitude. Furthermore, we show the model can be further improved using machine learning and statistical inference methods that integrate additional material properties.

Received 1st July 2021,
Accepted 5th September 2021

DOI: 10.1039/d1cy01170g

rsc.li/catalysis

Hydrogen is a powerful energy carrier that can be generated through the hydrogen evolution reaction (HER) – the critical cathodic reaction of electrochemical water-splitting. Not surprisingly, the HER is still a topic of great fundamental interest for electrochemical energy conversion.[1–9] To understand the HER activity, Bockris,[10] Conway and Bockris,[11] Petrenko,[12] Kita[13] and Trasatti[14–16] correlated experimental HER reaction rates with physicochemical descriptors such as atomic number, work function, d-band center, the heat of hydrogen adsorption, and Pauling electronegativities. Motivated by Sabatier's principle that the maximum catalytic rate is achieved when the interaction between the reactants and catalyst is neither too strong nor too weak,[17] Parsons and Gerischer independently proposed the free energy of hydrogen adsorption, Δg^0, as an HER descriptor such that the maximum rate corresponds to a minimum in the magnitude of Δg^0 under equilibrium conditions.[18,19] To link the theoretical Δg^0 with experimental measurements, early attempts were made by Trasatti.[15] Later, Krishtalik[20] and Trasatti[15] used a compilation of experimental data to validate the Parsons volcano relationship using the metal-hydrogen interaction strength based on the Eley–Stevenson method.[21,22] However, this approach had limited success because the maximum exchange current was not associated with $\Delta g^0 = 0$, as proposed by Parsons.

In a seminal study, Nørskov and collaborators introduced the hydrogen adsorption free energy ΔG_H computed from density functional theory (DFT) as an accurate estimate of Parsons' Δg^0. Further, this study built a connection with electrochemical exchange currents using a simple kinetic model based on systematic investigations on transition metal surfaces.[23] We will refer to this model as the Nørskov model hereafter. The Nørskov model confirms the theoretical volcano trend proposed by Parsons where $\Delta G_H \approx 0$ at the maximum exchange current density of the HER. Further, this model also demonstrated that a computational framework based on an easy-to-compute descriptor ΔG_H can provide a rational approach to catalyst design, which improved on approaches to materials design based on trial-and-error or chemical heuristics that have historically been the norm for experimental catalysis research.

Although the Nørskov model for the HER has been widely accepted by the electrochemistry community (*e.g.*, see recent studies[24–27]), several studies highlighted caveats in this model. For example, the Nørskov model is applied to pristine metallic surfaces to compute ΔG_H while under electrochemical conditions, many metals are likely to be oxidized or exhibit amorphous surface structure.[28–30] Further, it was argued that the electrostatic effects from metal–water interfaces and the effects from the adsorption of water and oxygen, as well as kinetic factors and d-band characteristics, are not adequately accounted for in the Nørskov model.[28–30] In addition, it has been recently argued that Pt is not a

[a] *Department of Mechanical Engineering and Materials Science, University of Pittsburgh, Pittsburgh, PA 15260, USA. E-mail: alsaidi@pitt.edu*
[b] *Department of Chemical and Petroleum Engineering, University of Pittsburgh, Pittsburgh, PA 15260, USA*

† Electronic supplementary information (ESI) available. See DOI: 10.1039/d1cy01170g

thermoneutral catalyst with ΔG_H that deviates from zero.[31–33] Several studies proposed HER models based on microkinetic analysis.[34,35] However, these models are generally complex with many parameters that are obtained by some approximation for by fitting to experimental data. *These caveats notwithstanding, the Nørskov model remains a leading framework for the design of HER catalysts and heterogeneous electrocatalysts in general.*[1–5]

Herein we revisit the Nørskov model and show that the calculated exchange current densities deviate from the corresponding experimental values by up to six orders of magnitude.[23] While differences between experimental and DFT-computed rates are not uncommon, we show that the discrepancy can be substantially reduced by considering that the rate constant is material-dependent rather than universal, as assumed in the original Nørskov model.[23] Specifically, we present evidence that the kinetic pre-factor k_0 also depends on the absolute value of ΔG_H. We further validate the findings based on reliable data obtained from a critical review of experimental exchange current densities on transition metal surfaces from the available research literature.

In the Nørskov model, the exchange current density j_0, which describes the magnitude of the forward and reverse reaction rates at equilibrium, is defined as

$$j_0 = \begin{cases} ek_0 \exp(-\Delta G_H/k_B T) C_{tot}(1-\theta) & \text{for } \Delta G_H > 0 \\ ek_0 C_{tot}(1-\theta) & \text{for } \Delta G_H < 0 \end{cases}, \quad (1)$$

where e is the charge of an electron and C_{tot} is the areal concentration of adsorption sites. Note that while the Nørskov model was presented in terms of the exchange current (*e.g.*, amps), eqn (1) is defined in terms of the exchange current density (*e.g.*, amps per square cm), which necessitates the inclusion of an area-normalized C_{tot}. The model is derived from the basic relation that the current is linearly proportional to the concentration of reactants H^+ (H*) for $\Delta G_H > 0$ ($\Delta G_H < 0$). Further, k_0 encompasses several factors such as additional concentration factors due to applied and formal potentials, reaction rates for all elementary steps, and the effects from transfer coefficients in microkinetic models.[34–36] Based on *ab initio* thermodynamic analysis,[37,75] we assume that the hydrogen coverage is at the lowest limit for metal surfaces that repel hydrogen (*i.e.*, with $\Delta G_H > 0$), and attains a full monolayer coverage for surfaces that are attractive to hydrogen (*i.e.*, with $\Delta G_H < 0$). At a given temperature T, the fraction of surface occupied sites by hydrogen follows the Langmuir model such that $\theta = K/(1+K)$ with $K = \exp(-\Delta G_H/k_B T)$. k_0 is the rate constant that is assumed to have a universal value for all metals, which is taken as $k_0 = 200\ s^{-1}\ site^{-1}$ by linearly fitting exchange currents to experimental data.[23] In a previous study we have shown that k_0 assumes a different value for β-Mo_2C nanoparticles by fitting to experimental results.[38]

The hydrogen adsorption free energy ΔG_H is obtained from the free energy difference between the hydrogen in gas phase and in adsorbed phase, which can be computed as,

$$\Delta G_H = \Delta E_{ads} + \Delta E_{ZPE} - T\Delta S, \quad (2)$$

where ΔE_{ZPE} is the zero-point energy that is found to be less than 0.05 eV for all metals, consistent with prior results.[23] ΔS is the entropy between the hydrogen adsorbed state and the gas state. It can be approximated as $-\frac{1}{2}S^0_{H_2}$ where $S^0_{H_2} = 1.35 \times 10^{-3}$ eV K^{-1} is the entropy of hydrogen in the gas phase at room temperature, as obtained from experimental measurements.[39] The hydrogen adsorption energy ΔE_{ads} is defined as,

$$\Delta E_{ads} = \frac{1}{n}\left(E_{slab/nH^*} - E_{slab} - \frac{n}{2}E_{H_2}\right), \quad (3)$$

where n is the number of adsorbed hydrogen atoms, E_{slab/nH^*} and E_{slab} are the energies of the slab with n adsorbed hydrogen atoms (H*) and of a clean slab respectively, and E_{H_2} is the energy of H_2 in gas phase. All terms in eqn (3) are directly computed from DFT. The Nørskov model of eqn (1) shows that the maximum catalytic activity is at $\Delta G_H = 0$ and the activity decreases when ΔG_H moves away from zero, thus reproducing the volcano relationship for exchange current and adsorption free energy ΔG_H.

The data labeled "Nørskov Model/Nørskov Data" in Fig. 1 shows the experimental exchange current densities j_0 obtained from the original report *vs.* the computed values based on the Nørskov model. For consistency, we use the same ΔG_H values as in the original report to compute j_0 from eqn (1). As seen in Fig. 1, the Nørskov model qualitatively captures the experimental trend for the currents among the different metals. However, the model underestimates the experimental exchange currents by 3–6 orders of magnitude for the metal surfaces with low HER activity such as W, Nb, Au, and Ag, while it is in better agreement (within two orders of magnitude) for the highly catalytic surfaces of Pt, Pd, Ir, and Rh. We further confirm that the underestimation of exchange currents on low activity surfaces is not due to experimental errors. For example, for Bi, In and Cd, the experimental values are $\sim 10^{-10}$ A cm^{-2} that we have carefully examined from available literature (see Table S5†). In contrast, the corresponding exchange currents obtained from Nørskov model are $\sim 10^{-21}$, $\sim 10^{-17}$ and $\sim 10^{-19}$ A cm^{-2}, respectively. The large discrepancy between experimental and theoretical predictions, in addition to the systematic variation in the discrepancy, strongly suggests that the model does not capture one or more relevant physical parameters.

In the Nørskov model, the rate constant k_0 is assumed to be constant for all metals, which was justified considering that k_0 includes mainly effects of solvent reorganization during proton transfer to electrode surfaces. However, this approximation is too simplistic given the significant differences in the HER kinetics between highly efficient

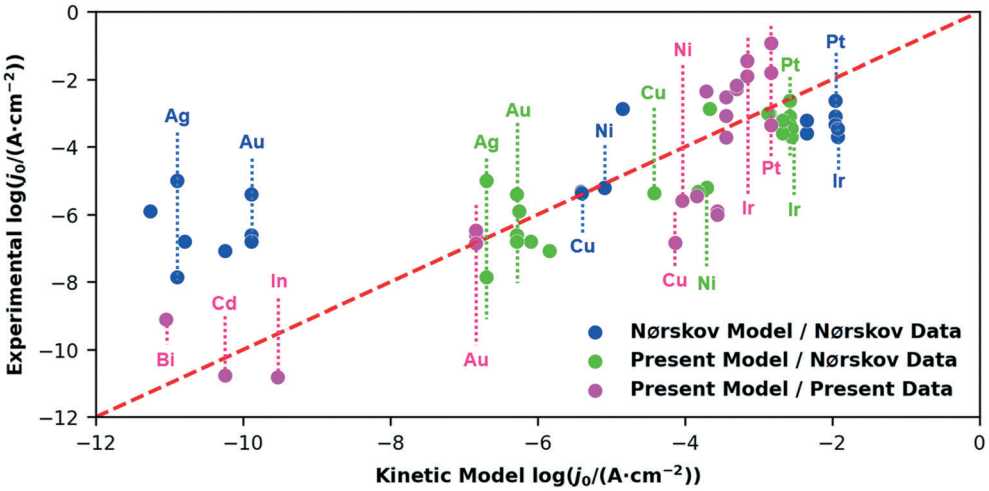

Fig. 1 Comparison of experimental and calculated exchange current densities. We use the experimental data provided from the original work of ref. 23 (Nørskov data) and our database of Table 1 (present data). The models from the original work (Nørskov model) and our modified model (present model) are used for the calculation of j_0. To avoid clutter, we only labeled few elements belonging to three categories that are excellent (Pt and Ir), moderate (Ni and Cu) and poor (Ag, Au, Bi, In and Cd) HER catalysts. All data are shown in Table S3.†

surfaces such as Pt and Ir, and surfaces with lower HER activity such as W and Ag. For example, a very weak H-binding surface is likely to have a transition state that is similar in nature to a surface-bound hydrogen (the Volmer reaction as the rate-determining step), whereas a strong H-binding surface is likely to have a transition state that resembles H^+ in the electrolyte or a weakly bound H_2 (the Heyrovsky or the Tafel reaction is rate-determining). Thus, outer-sphere effects that can be rationalized as the reorganization of solvents[40] may be more significant for strong H-binding surfaces than weak H-binding surfaces.[41] Further, other factors contribute to different HER dynamics between metal surfaces, such as the solution pH and the composition and structure of the double layer, particularly for inefficient catalysts that require very large overpotentials (and commensurately large electric fields across the double layer) to drive the HER.[42]

Re-examining the data provided in the original report,[23] our analyses clearly show that a universal k_0 value is not justified. Fig. 2 presents implied k_0 values obtained from linear regression analysis of eqn (1) using experimental j_0 values and the DFT computed ΔG_H. This approach amounts to testing the hypothesis that deviations between the experimental and DFT-predicted j_0 using the Nørskov model can be attributed to a metal-dependent value of k_0. As seen in the figure, for both low and high coverage limits, k_0 varies systematically with ΔG_H over several orders of magnitude, where metals that weakly interact with hydrogen have low k_0

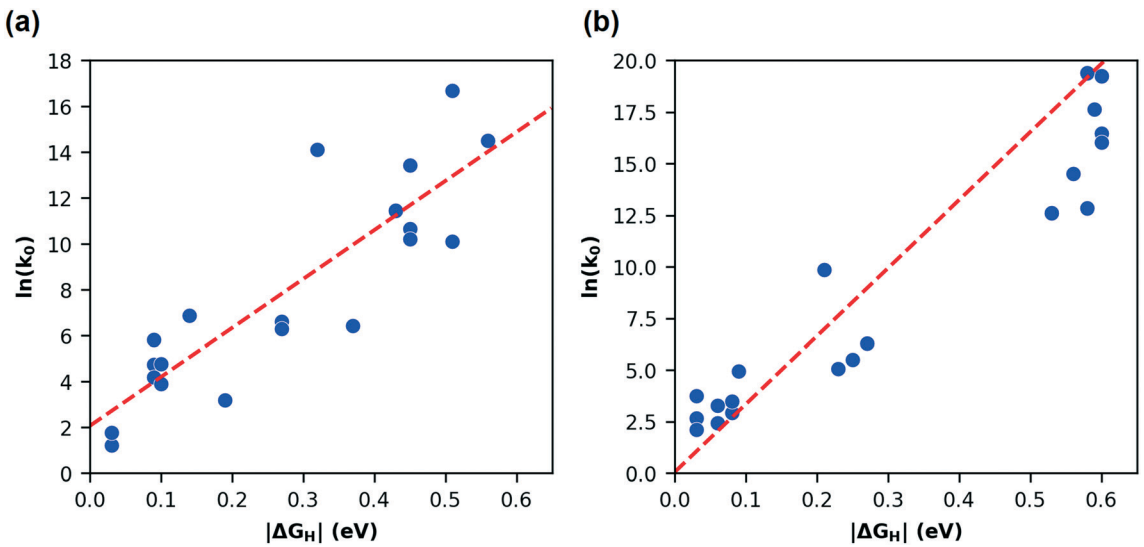

Fig. 2 The correlation of ln(k_0) *vs.* absolute value for the hydrogen adsorption free energy $|\Delta G_H|$ calculated from DFT for (a) low- and (b) high-coverage limits. All data including experimental currents and computed ΔG_H are from ref. 23.

values and those that strongly interact with hydrogen, either repulsive or attractive, have larger k_0 values. Further, as shown in Fig. 2, we find a strong linear correlation between $\ln(k_0)$ and $|\Delta G_H|$. Indeed, invoking this linear relationship is found to substantially decrease the inconsistency between the kinetic model and the experimental values, as shown in Fig. 1 for the data labeled "Present Model/Nørskov Data". We conclude from the analysis based on data in ref. 23 that k_0 is not universal but is material-specific, at least to the extent that efficient *versus* inefficient metals should exhibit characteristically different k_0 values. Notably, when restricted to a model that only incorporates metals with a similar range of H-binding energies, this effect is diminished – hence the fit is relatively good near the peak of the volcano only.

Recently, the Brønsted–Evans–Polanyi (BEP) relation, a linear relation between a reaction's free energy and its activation energy E_a, is confirmed for the HER on pure metal surfaces[43] using a computational approach that corrects for finite-size effects in periodic supercell simulations. For example, for the metals with $\Delta G_H < 0$ ($\Delta G_H > 0$), the activation barrier of the rate-limiting Heyrovsky (Volmer) reaction decreases with increasing (decreasing) ΔG_H. The BEP relation on HER is also confirmed experimentally on precious metals of Pt, Ir, Pd and Rh.[44] If we assume that k_0 of the Nørskov model is the HER reaction rate constant which follows the Arrhenius relation that $\ln(k_0)$ is linearly proportional to activation energy E_a, and is in conjunction with the BEP relationship, we can infer the linear dependence between $\ln(k_0)$ and $|\Delta G_H|$ that is obtained using our data-driven approach. Further, the enthalpy–entropy compensation where E_a (or ΔG_H) has a linear relationship with entropy[45] suggests that $\ln(k_0)$ includes effects from activation entropy that is metal-dependent,[46] which also supports our findings. However, we believe that a careful derivation is needed to formally derive the dependence between k_0 and E_a.

To further examine the metal-dependence of k_0, we have compiled an additional set of experimental j_0 values from a thorough literature search in Table 1 (see comments and references in Table S5†) and re-analyzed ΔG_H using different DFT functionals (see Table S2†). The comparison between the experimental values and the values conputed from the present model are shown in Fig. 1 under "Present Model/Present Data". Fig. 3(a) shows the correlation between $\ln(k_0)$ and $|\Delta G_H|$ and Fig. 3(b) shows the volcano relationship corresponding to the new data. The DFT calculations are carried out using the Vienna *ab initio* simulation package (VASP).[47–49] More details about the DFT computational framework are provided in the ESI.† We employ the conventional[50] (PBE) and revised[51] (RPBE) Perdew–Burke–Ernzerhof exchange–correlational functional with and without van der Waals (vdW) corrections[52,53] to assess the variability of the results with the computational framework. The results shown in Fig. 1 and 3 are based on RPBE + vdW; however, the findings are found not to be sensitive to the functional (see Table S2†).

Table 1 The collected exchange current densities from experiments

Electrode	Reported j_0 (A cm^{-2})	Electrolyte	Temperature	Ref.
Pt (111)	4.5×10^{-4}	0.05 M H_2SO_4	303 K	54
Pt (100)	6.0×10^{-4}			
Pt (110)	9.8×10^{-4}			
Pt/C	1.6×10^{-2}	0.2 M H_3PO_4	293 K	55
Pt/C	1.2×10^{-1}	0.1 M $HClO_4$	313 K	56
Ir/C	3.6×10^{-2}	0.1 M $HClO_4$	313 K	56
Ir/C	1.28×10^{-2}	0.2 M H_2SO_4	293 K	55
Pd	1.9×10^{-4}	0.5 M H_2SO_4	Not mentioned	57
Pd/C	3.0×10^{-3}	0.1 M $HClO_4$	313 K	56
Pd/C	8.4×10^{-4}	0.1 M $HClO_4$	293 K	55
Rh/C	5.2×10^{-3}	0.1 M $HClO_4$	313 K	56
Rh/C	6.7×10^{-3}	0.1 M $HClO_4$	293 K	55
Ru	4.5×10^{-3}	1 M HCl + NaCl	298 K	58
Cu	1.45×10^{-7}	0.1 N HCl	Not mentioned	59
Co	3.6×10^{-6}	1 M H_2SO_4	293 K	60
Ni	2.6×10^{-6}	0.5 M H_2SO_4	295 K	61
Au (111)	2.5×10^{-7}	0.1 M $HClO_4$	Not mentioned	62
Au (100)	0.5×10^{-7}			
Au (110)	0.3×10^{-7}			
Au (111)	3.38×10^{-7}	0.5 M H_2SO_4	Not mentioned	63
Poly Au	1.40×10^{-7}	0.1 M $HClO_4$	Not mentioned	62
Re	1.25×10^{-6}	0.5 M H_2SO_4	298 K	64
Re	1×10^{-6}	0.5 M H_2SO_4	298 K	65
Cd	1.7×10^{-11}	0.5 N H_2SO_4	Not mentioned	66
Bi	8×10^{-10}	4.8 M H_2SO_4	Not mentioned	67
In	1.51×10^{-11}	0.1 M $HClO_4$	303 K	68

The library of experimental exchange current densities[54–68] labeled as "Present Data" in Fig. 1 and used in Fig. 3 was collected from a larger set of prior literature reports, which were then down-selected to only those reports that minimized or otherwise accounted for the impacts of electrolyte/surface contamination, electrode roughness, and mass transfer effects. Table 1 summarizes the experimental results. A detailed discussion of this down-selection process is included in the ESI.† We also chose to exclude metals that are expected to be oxidized under HER conditions in acidic solution, such as Mo, W, and Nb.[69] Finally, we added measurements on Cd, In, and Bi and Ru that were not included in ref. 23. Fig. 3 shows that considerably more experimental data are available for HER-active metals, which accounts for the greater density of points with small $|\Delta G_H|$. The spread in these data likely reflects uncertainty both in DFT-calculated ΔG_H and experimental j_0.[70] Nonetheless, as shown in Fig. 3(a), there is a clear linear relationship between $\ln k_0$ and $|\Delta G_H|$ that can be described as $\ln(k_0) = 23.16|\Delta G_H| + 3.17$. This is specifically evidenced in clustering of three metal groups with characteristically different H binding energies: the precious metals (Pt, Ir, Pd and Rh) near $|\Delta G_H| = 0.1$ eV, the metals near $|\Delta G_H| = 0.5$ eV, and the HER inert metals near $|\Delta G_H| = 1$ eV.

Our results clearly show that ΔG_H more accurately describes j_0 for the HER if we include an additional exponential relationship between $|\Delta G_H|$ on k_0. However, it is conceivable that k_0, and hence the exchange current density, also depends on other metal properties besides ΔG_H. For instance, previous studies postulated that the HER rate can

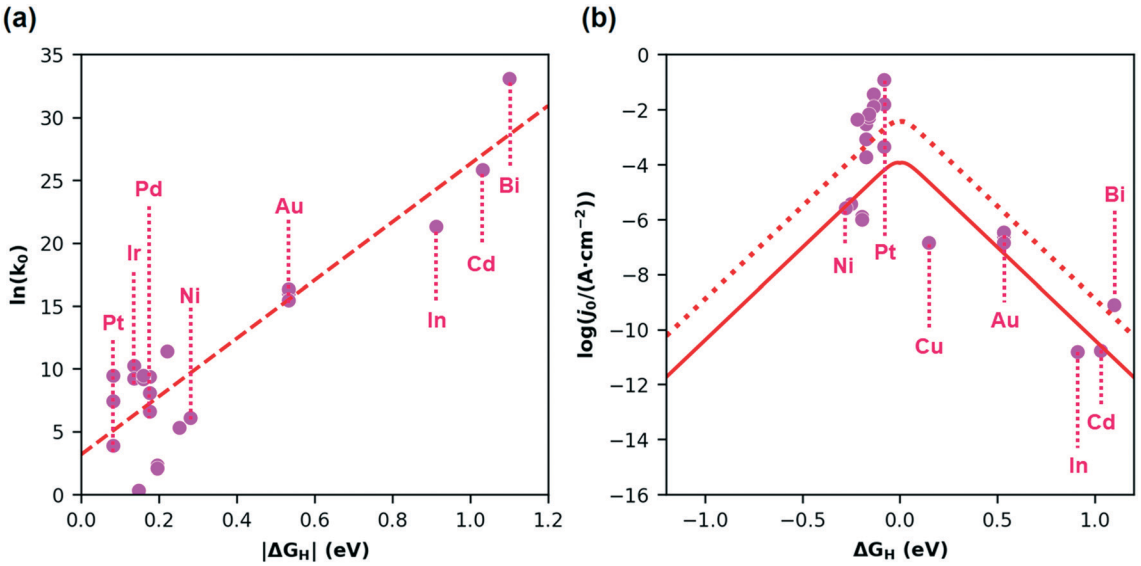

Fig. 3 (a) Correlation between $\ln(k_0)$ and $|\Delta G_H|$ using "Present Data" of Fig. 1 (see Table S4†). From the linear fitting, we obtain $\ln(k_0) = 23.16|\Delta G_H| + 3.17$ with a correlation factor of $r^2 = 0.82$. (b) The new volcano curve of j_0 based on the present model/present data. The dotted and solid red lines are obtained using eqn (1) with the maximum and the minimum C_{tot} in our data, respectively.

be modeled by using atomic number, work functions, and Pauling electronegativities as material descriptors.[10–16] To investigate this, we used a machine learning approach based on SISSO (sure independence screening and sparsifying operator)[71–74] to develop an accurate and physically interpretable model for $\ln k_0$. We investigated the following primary atomic features in this analysis: empirical radius, mass, number, period in periodic table, electron affinity, ionization energy, and Pauling electronegativity, in addition to the following metal features: density and work function. In the SISSO approach, potential descriptors for $\ln k_0$ are formed from the primary features with up to ten level interactions of complexity utilizing three mathematical operations (addition, multiplication, and division). The limited size of the experimental dataset (12 metals) precludes a full investigation, and thus, we used a relatively small number of primary features and mathematical operations in the construction of only one-dimensional descriptors. By searching the massive space of potential descriptors, SISSO identified many models for $\ln k_0$ that capture a large proportion of the variations among different elements. Table S6† lists the best ten models with correlation coefficients $r^2 > 0.975$. Notably all these models are found to depend on $|\Delta G_H|$ indicating its prime effect on k_0. However, a larger experimental database is needed to unambiguously validate the findings, and to identify other, if any, important material properties that affect k_0.

In summary, we agree with the original work by Nørskov and collaborators that the trend of j_0 can be explained by a kinetic model that relies on ΔG_H as the sole descriptor. However, after carefully analyzing the experimental and computational results, we propose that the same kinetic model better matches with experiments over a wide range of metals by treating the logarithm of the rate constant k_0 as a linear function of the absolute value of ΔG_H.

Conflicts of interest

There are no conflicts to declare.

Acknowledgements

W. A. S. and T. Y. acknowledge partial financial support from the National Science Foundation (Award No. DMR-1809085). R. B. P. and J. R. M. acknowledge the Arnold and Mabel Beckman Foundation for financial support *via* the Beckman Young Investigator program. We are grateful for computing time provided in part by the CRC resources at the University of Pittsburgh and Argonne Leadership Computing Facility, which is a DOE Office of Science User Facility supported under Contract DE-AC02-06CH11357.

References

1 Z. W. Seh, J. Kibsgaard, C. F. Dickens, I. Chorkendorff, J. K. Nørskov and T. F. Jaramillo, *Science*, 2017, **355**, eaad4998.
2 J. Greeley, *Annu. Rev. Chem. Biomol. Eng.*, 2016, **7**, 605–635.
3 M. T. M. Koper, *Chem. Sci.*, 2013, **4**, 2710–2723.
4 J. K. Nørskov, T. Bligaard, J. Rossmeisl and C. H. Christensen, *Nat. Chem.*, 2009, **1**, 37–46.
5 J. K. Nørskov, F. Abild-Pedersen, F. Studt and T. Bligaard, *Proc. Natl. Acad. Sci. U. S. A.*, 2011, **108**, 937.
6 S. B. Scott, A. K. Engstfeld, Z. Jusys, D. Hochfilzer, N. Knøsgaard, D. B. Trimarco, P. C. K. Vesborg, R. J. Behm and I. Chorkendorff, *Catal. Sci. Technol.*, 2020, **10**, 6870–6878.
7 S. Mansingh, K. K. Das and K. Parida, *Sustainable Energy Fuels*, 2021, **5**, 1952–1987.

8 M. Z. Rahman, M. G. Kibria and C. B. Mullins, *Chem. Soc. Rev.*, 2020, **49**, 1887–1931.
9 T. T. Yang, T. L. Tan and W. A. Saidi, *Chem. Mater.*, 2020, **32**, 1315–1321.
10 J. O. M. Bockris, *Trans. Faraday Soc.*, 1947, **43**, 417–429.
11 B. E. Conway and J. O. M. Bockris, *J. Chem. Phys.*, 1957, **26**, 532–541.
12 A. T. Petrenko, *Zh. Fiz. Khim.*, 1965, **39**, 2097.
13 H. Kita, *J. Electrochem. Soc.*, 1966, **113**, 1095.
14 S. Trasatti, *J. Electroanal. Chem. Interfacial Electrochem.*, 1971, **33**, 351–378.
15 S. Trasatti, *J. Electroanal. Chem. Interfacial Electrochem.*, 1972, **39**, 163–184.
16 S. Trasatti, *J. Chem. Soc., Faraday Trans. 1*, 1972, **68**, 229–236.
17 P. Sabatier, *La Catalyse en Chimie Organique, Encyclopédie de Science Chimique Appliquée*, Dunham, QC: Ch. Béranger, 1913.
18 R. Parsons, *Trans. Faraday Soc.*, 1958, **54**, 1053–1063.
19 H. Gerischer, *Bull. Soc. Chim. Belg.*, 1958, **67**, 506–527.
20 P. Delahay and C. W. Tobias, *Advances in electrochemistry and electrochemical engineering*, Interscience Publishers, 1970, vol. 7, p. 283.
21 D. D. Eley, *Discuss. Faraday Soc.*, 1950, **8**, 34–38.
22 D. P. Stevenson, *J. Chem. Phys.*, 1955, **23**, 203–203.
23 J. K. Nørskov, T. Bligaard, A. Logadottir, J. R. Kitchin, J. G. Chen, S. Pandelov and U. Stimming, *J. Electrochem. Soc.*, 2005, **152**, J23–J26.
24 P. V. Sarma, T. V. Vineesh, R. Kumar, V. Sreepal, R. Prasannachandran, A. K. Singh and M. M. Shaijumon, *ACS Catal.*, 2020, **10**, 6753–6762.
25 J. D. Benck, T. R. Hellstern, J. Kibsgaard, P. Chakthranont and T. F. Jaramillo, *ACS Catal.*, 2014, **4**, 3957–3971.
26 C. Li, Z. Chen, H. Yi, Y. Cao, L. Du, Y. Hu, F. Kong, R. Kramer Campen, Y. Gao, C. Du, G. Yin, I. Y. Zhang and Y. Tong, *Angew. Chem., Int. Ed.*, 2020, **59**, 15902–15907.
27 E. M. Lopato, E. A. Eikey, Z. C. Simon, S. Back, K. Tran, J. Lewis, J. F. Kowalewski, S. Yazdi, J. R. Kitchin, Z. W. Ulissi, J. E. Millstone and S. Bernhard, *ACS Catal.*, 2020, **10**, 4244–4252.
28 R. Kronberg and K. Laasonen, *J. Phys. Chem. C*, 2020, **124**, 13706–13714.
29 N. Holmberg and K. Laasonen, *J. Phys. Chem. C*, 2015, **119**, 16166–16178.
30 G. Kastlunger, P. Lindgren and A. A. Peterson, *J. Phys. Chem. C*, 2018, **122**, 12771–12781.
31 P. Lindgren, G. Kastlunger and A. A. Peterson, *ACS Catal.*, 2020, **10**, 121–128.
32 R. Kronberg and K. Laasonen, *ACS Catal.*, 2021, 8062–8078, DOI: 10.1021/acscatal.1c00538.
33 H. Ooka, M. E. Wintzer and R. Nakamura, *ACS Catal.*, 2021, **11**, 6298–6303.
34 A. R. Kucernak and C. Zalitis, *J. Phys. Chem. C*, 2016, **120**, 10721–10745.
35 H. Ooka and R. Nakamura, *J. Phys. Chem. Lett.*, 2019, **10**, 6706–6713.
36 T. Shinagawa, A. T. Garcia-Esparza and K. Takanabe, *Sci. Rep.*, 2015, **5**, 13801.
37 E. Skúlason, V. Tripkovic, M. E. Björketun, S. Gudmundsdóttir, G. Karlberg, J. Rossmeisl, T. Bligaard, H. Jónsson and J. K. Nørskov, *J. Phys. Chem. C*, 2010, **114**, 18182–18197.
38 T. T. Yang and W. A. Saidi, *Nanoscale*, 2017, **9**, 3252–3260.
39 M. W. Chase, Jr, *J. Phys. Chem. Ref. Data, Monogr.*, 1998, 1–1951.
40 R. A. Marcus, *Rev. Mod. Phys.*, 1993, **65**, 599–610.
41 R. Kant, J. Kaur and G. K. Mishra, *J. Phys. Chem. C*, 2020, **124**, 2273–2288.
42 H. Shi, Z. Cai, J. Patrow, B. Zhao, Y. Wang, Y. Wang, A. Benderskii, J. Dawlaty and S. B. Cronin, *ACS Appl. Mater. Interfaces*, 2018, **10**, 33678–33683.
43 M. T. Tang, X. Liu, Y. Ji, J. K. Norskov and K. Chan, *J. Phys. Chem. C*, 2020, **124**, 28083–28092.
44 J. Zheng, W. Sheng, Z. Zhuang, B. Xu and Y. Yan, *Sci. Adv.*, 2016, **2**, e1501602.
45 S. Gelin, A. Champagne-Ruel and N. Mousseau, *Nat. Commun.*, 2020, **11**, 3977.
46 T. Shinagawa and K. Takanabe, *J. Phys. Chem. C*, 2016, **120**, 24187–24196.
47 J. F. G. Kresse, *Phys. Rev. B: Condens. Matter*, 1996, **54**, 11169.
48 M. Shishkin, M. Marsman and G. Kresse, *Phys. Rev. Lett.*, 2007, **99**, 246403.
49 G. Kresse and D. Joubert, *Phys. Rev. B: Condens. Matter Mater. Phys.*, 1999, **59**, 1758.
50 J. P. Perdew, K. Burke and M. Ernzerhof, *Phys. Rev. Lett.*, 1996, **77**, 3865.
51 J. P. Perdew, K. Burke and M. Ernzerhof, *Phys. Rev. Lett.*, 1996, **77**, 3865–3868.
52 A. Tkatchenko and M. Scheffler, *Phys. Rev. Lett.*, 2009, **102**, 073005.
53 W. Al-Saidi, V. K. Voora and K. D. Jordan, *J. Chem. Theory Comput.*, 2012, **8**, 1503–1513.
54 N. M. Marković, B. N. Grgur and P. N. Ross, *J. Phys. Chem. B*, 1997, **101**, 5405–5413.
55 J. Zheng, W. Sheng, Z. Zhuang, B. Xu and Y. Yan, *Sci. Adv.*, 2016, **2**, e1501602.
56 J. Durst, C. Simon, F. Hasché and H. A. Gasteiger, *J. Electrochem. Soc.*, 2014, **162**, F190–F203.
57 W. Xu, S. Zhu, Y. Liang, Z. Cui, X. Yang, A. Inoue and H. Wang, *J. Mater. Chem. A*, 2017, **5**, 18793–18800.
58 A. T. Kuhn and P. M. Wright, *J. Electroanal. Chem. Interfacial Electrochem.*, 1970, **27**, 319–323.
59 N. Pentland, J. O. M. Bockris and E. Sheldon, *J. Electrochem. Soc.*, 1957, **104**, 182.
60 A. T. Kuhn, C. J. Mortimer, G. C. Bond and J. Lindley, *J. Electroanal. Chem. Interfacial Electrochem.*, 1972, **34**, 1–14.
61 E. Navarro-Flores, Z. Chong and S. Omanovic, *J. Mol. Catal. A: Chem.*, 2005, **226**, 179–197.
62 J. Perez, E. R. Gonzalez and H. M. Villullas, *J. Phys. Chem. B*, 1998, **102**, 10931–10935.
63 S. Štrbac, I. Srejić and Z. Rakočević, *J. Electrochem. Soc.*, 2018, **165**, J3335–J3341.
64 J. G. Rivera, R. Garcia-Garcia, E. Coutino-Gonzalez and G. Orozco, *Int. J. Hydrogen Energy*, 2019, **44**, 27472–27482.

65 R. Garcia-Garcia, G. Ortega-Zarzosa, M. E. Rincón and G. Orozco, *Electrocatalysis*, 2015, **6**, 263–273.
66 J. O. M. Bockris and S. Srinivasan, *Electrochim. Acta*, 1964, **9**, 31–44.
67 Y. M. Wu, W. S. Li, X. M. Long, F. H. Wu, H. Y. Chen, J. H. Yan and C. R. Zhang, *J. Power Sources*, 2005, **144**, 338–345.
68 J. N. Butler and M. Dienst, *J. Electrochem. Soc.*, 1965, **112**, 226.
69 M. Pourbaix, *Atlas of Electrochemical Equilibria in Aqueous Solutions*, National Association of Corrosion Engineers, 1974.
70 D. Krishnamurthy, V. Sumaria and V. Viswanathan, *J. Phys. Chem. Lett.*, 2018, **9**, 588–595.
71 M. Andersen, S. V. Levchenko, M. Scheffler and K. Reuter, *ACS Catal.*, 2019, **9**, 2752.
72 A. Mazheika, Y. Wang, R. Valero, L. M. Ghiringhelli, F. Viñes, F. Illas, S. V. Levchenko and M. Scheffler, 2021.
73 L. M. Ghiringhelli, J. Vybiral, S. V. Levchenko, C. Draxl and M. Scheffler, *Phys. Rev. Lett.*, 2015, **114**, 105503.
74 L. M. Ghiringhelli, J. Vybiral, E. Ahmetcik, R. Ouyang, S. V. Levchenko, C. Draxl and M. Scheffler, *New J. Phys.*, 2017, **19**, 023017.
75 T. T. Yang and W. A. Saidi, *J. Phys. Chem. Lett.*, 2020, **11**, 2759–2764.

